PSPMT and PIN Diode Designs of a Small Scintillation Camera for Imaging Malignant Breast Tumors

Craig S. Levin, Edward J. Hoffman, Martin P. Tornai, and Lawrence R. MacDonald

Division of Nuclear Medicine and Biophysics, UCLA School of Medicine
Los Angeles, CA 90095-6948

Abstract

We are investigating the concept of utilizing a small gamma ray scintillation camera to help identify and localize malignant breast tumors after a suspicious finding in a mammogram. We are exploring two different photodetector technologies for a small prototype camera development. The first uses a position sensitive photomultiplier (PSPMT) as the photodetector, the second, an array of silicon PIN diodes (PD). In this report, we present imaging results obtained with a NaI(Tl)-PSPMT design, and the design features, expected performance and relevant energy measurements obtained for the CsI(Tl)-PD based device.

I. INTRODUCTION

Mammography is accepted as the best means of screening for non-palpable breast cancer. However, while the sensitivity of mammography is on the order of 85% for detecting signatures of breast cancer, those signatures are only 20-30% specific to malignancy. The result is a 70-80% rate of false positives and a large number of unnecessary biopsies. Recent reports on detection of malignant breast tumors using ^{99m}Tc-Sestamibi and Methylene Diphosphonate (MDP) all give sensitivities and specificities of 90% or better. We believe it is possible to take advantage of this high sensitivity and specificity to reduce the number of unnecessary biopsies if an appropriate scintillation camera were available in or near the mammography suite. Unfortunately, because of its size (~50-70 cm across), the standard scintillation camera is not ideal for breast imaging, particularly in the confined area of a mammography suite. It has been shown that a portion of the roughly 10% of lesions missed in ^{99m}Tc- Sestamibi studies cited above can be explained by either a small size and/or lower isotope uptake of the particular lesions, tissue attenuation or myocardial background. Such problems could be remedied in part by a dedicated small higher resolution camera which can image the breast in close proximity at angles that avoid background from the rest of the body.

Our initial test device has a 6 cm x 6 cm field of view (FOV), a size compatible with standard mammography fixtures for compressing and immobilizing breasts during tumor localization or core biopsy. Ideally, the placement of the camera over a lesion would be guided by mammography. If the small camera is used in conjunction with mammographic breast-compression, the resolution and signal-to-noise ratio (SNR) should be better than that attainable with conventional scintillation cameras due to less gamma ray attenuation. Once the utility is verified, larger versions could be built.

We are exploring two photodetector technologies for this investigation of small scintillation cameras. Both schemes are essentially a miniaturization of the gamma ray camera concept. The first design employs a NaI(Tl) crystal coupled to a Position Sensitive Photomultiplier Tube (PSPMT). The second uses CsI(Tl) coupled to silicon PIN photodiodes (PD).

Other work on small camera development for scintillation breast imaging has been reported [1-4]. Small gamma ray cameras based on PSPMT technology have been under development by others for medical imaging, radiation monitoring and astrophysical applications [see 5-8]. Small cameras based on CsI(Tl)-PD technology have also been attempted for use in astrophysics [9-10].

The attractiveness of the PD design is in part due to its potential for compactness and low cost [11]. Including background shielding and readout electronics, the CsI(Tl)-PD camera would be roughly an 8 x 8 x 6 cm^3 box. The corresponding size for a PSPMT camera is, perhaps, 10 cm x 10 x cm x 15-20 cm. The compactness of the solid state design is ideal for breast imaging. Also attractive is the inevitable reduction in the cost of silicon-based products.

II. METHODS

A. The PSPMT Camera Design

We have built and are currently testing and optimizing a small scintillation camera comprising a 6 cm x 6 cm x 6 mm thick NaI(Tl) crystal coupled to a Hamamatsu R3941 PSPMT. We performed Monte Carlo studies using the DETECT optical photon tracking code [12] to determine the optimal crystal surface treatments and reflectors. The best uniformity in both resolution and sensitivity were obtained with the following conditions: (1) *Top of crystal (where photons enter)*: fine ground and painted with a white diffuse reflector; (2) *Sides of crystal:* polished and painted black (absorbing); (3) *Bottom of crystal (in contact with PSPMT):* polished. These conditions are consistent with those for conventional gamma ray cameras. A hermetically sealed NaI(Tl) crystal was acquired with the optimal surface treatments, a 3 mm glass window and a 0.5 mm thick aluminum housing.

The R3941 PSPMT has an bialkali photocathode active area of 77 mm x 77 mm, 16 stage fine mesh dynode structure, and a 16 x 18 cross wire anode with 3.7 mm pitch. The inner 60 mm x 60 mm area is the most useful area of the tube in terms of its linearity. The PSPMT was selected for high photocathode uniformity (maximum variation of 3:1). The NaI(Tl) crystal and the PSPMT were optically coupled with silicon-based grease. When a gamma ray interacts in the crystal, the scintillation light created will be spread within the NaI(Tl) crystal (index of refraction, n = 1.85), the 3 mm glass window (n = 1.5) of the crystal housing, and the 3 mm glass entrance window of the PSPMT. The light sharing among all of the anode wires facilitates the positioning of scintillation events in this technique. Charge spread for the mesh dynode design is significant and results in unwanted inter-channel crosstalk. The PSPMT was read out using standard resistive charge division which multiplexes the 34 cross wire anode channels into 4 signals, designated as X+, X-, Y+, and Y-. Those signals were readout individually through a four channel line driver/preamplifier board [13], shaped (1.5 μs shaping time), amplified with NIM and digitized with CAMAC electronics. The sum of those signals was used for the timing of the trigger to gate the ADCs. The position of an event in a given direction (X or Y) is then determined by a weighted mean of the signals.

0-7803-3534-1/97 10.00©1997IEEE

The camera was characterized using both ^{57}Co (122, 136 keV) and ^{99m}Tc (140 keV) gamma ray sources. Intrinsic position uniformity and resolution was measured by stepping a 1.2 mm slit source across the face of the camera in both the X and Y directions. The slit source was formed with two 2.0 cm thick lead bricks spaced 1.2 mm apart. 6 cm x 6 cm squares of various lengths were cut out of a standard low energy, high resolution (~1.3 mm diameter, 4 cm long hexagonal-hole) collimator and fixed to the top of the NaI(Tl)-PSPMT device. We acquired images by placing various phantoms on top of a 2 cm thick collimator piece.

We also investigated the use of an array of small, discrete, parallel piped crystals coupled to the PSPMT instead of one large, continuous crystal. This segmented crystal scheme has two obvious advantages over the large, continuous crystal design: (1) a gamma ray photoabsorption within a given individual crystal in the array will create scintillation photons that will be confined to that crystal and focused onto a small spot on the PSPMT face. Since fewer anode wires would be involved for positioning, this would improve the SNR compared to sharing the light among many anode wires; (2) Because the light transmission properties are approximately identical for all crystals within the segmented array, the positioning will be linear up to the edge of the FOV, unlike in the continuous crystal scheme. Disadvantages of the discrete crystal design compared to the continuous crystal design are (1) its lower sensitivity (due to the dead area between crystals); (2) the resolution is determined by the size of the crystal; higher resolution requires smaller crystals, and, therefore more crystals are required in the array to cover the same area; (3) a matching square hole collimator must be used.

B. The PD Camera Design

We also are exploring the possibility of using CsI(Tl) coupled to an array of PDs for the small camera. The potential use of solid state photodetectors allows further compactness for the imaging device. If PDs are used as photodetectors, CsI(Tl) is the ideal scintillator since it has an excellent emission spectrum match to the absorption spectrum of silicon (~75% QE at 530 nm). In addition, CsI(Tl) has 35 % higher light yield than NaI(Tl) and a 65% higher stopping power at 140 keV. The higher stopping power allows the use of thinner crystals, improving light spread localization and transmission, with no loss in sensitivity. CsI(Tl) crystals are relatively non-hygroscopic, making them much easier to handle, and no glass window is required. Compared to a PMT, the photodiode is more compact, has potentially smaller spacing between photodetectors and a factor of 3 higher quantum efficiency. These features of the CsI(Tl)-PD combination could potentially give this design a comparable sensitivity and energy resolution to the NaI(Tl)-PSPMT scheme. The PMT, however, has a clear advantage in SNR and gain.

For any PD-preamplifier combination, for the optimum SNR at the preamplifier input the PD terminal capacitance is kept to a minimum. In addition, the PD leakage current generally increases with area. These facts, combined with the merit of using arrays of small crystals, as discussed at the end of the last subsection, imply that the best SNR for a CsI(Tl)-PD imaging array is achieved when it is composed of tiny (≤2 mm) CsI(Tl) crystals coupled to correspondingly small PD array elements. However, to cover a 6 cm x 6 cm area with such a highly pixellated PD array requires a customized and expensive readout. In addition, it would require a mosaic of several PD arrays to cover that large an area which would introduce significant dead regions between arrays. Finally, a custom-made square hole collimator would be required to match the crystal sizes chosen. Therefore, our initial investigation will study a coarse PD array composed of individual, large area (~10 mm x 10 mm) elements. We will determine whether or not this "simple" design has sufficient SNR for high resolution imaging and, if not, estimate the improvements necessary.

A schematic for the "simple" device is shown in Figure 1. It utilizes a 5 x 5 array of 10 mm x 10 mm area PDs with 2 mm spacing between. Both continuous and discrete CsI(Tl) crystal array designs are shown. A light guide is used to distribute light over the coarse array of PDs. The PDs for the initial array we are proposing (Hamamatsu S3590) are readily available so that no custom PD array manufacturing is necessary.

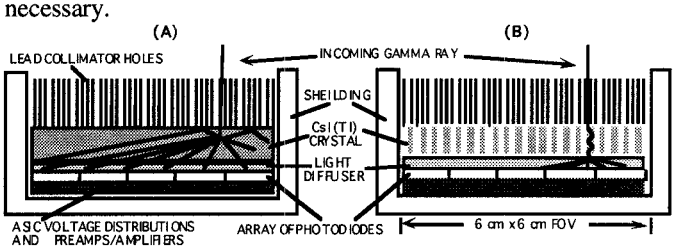

Figure 1. Schematic of the "simple" photodiode designs of a small, compact, gamma-ray scintillation camera for breast imaging. (a) Single continuous crystal. (b) Array of discrete crystals. Size: 8x8x6 cm^3, including background shielding.

Monte Carlo simulations were performed using DETECT optical photon tracking code for the continuous crystal design (Fig. 1a). A 140 keV gamma ray interaction in CsI(Tl) produces approximately 7300 photons with a peak emission wavelength of 530 nm. These optical photons were tracked and optimal crystal surface treatments and reflectors were determined. The best uniformity in resolution and sensitivity was obtained with the same surface treatments as found for the NaI(Tl) (see previous section). Under these optimal conditions, light tracking simulations were then used to determine camera characteristics, such as, the light transmission, the thickness of the light diffuser, the light spread aperture, the positioning linearity and resolution and depth of interaction effects.

Energy measurements were made with various gamma ray sources and a small 2x2x10 mm^3 CsI(Tl) crystal coupled to one of the proposed PDs. The crystal was wrapped in 5 layers of teflon and coupled to the PD with optical grease. The PD was readout with a charge sensitive preamplifier (ORTEC 142A), a shaping amplifier (CANBERRA 2021, gaussian, 1.5μs shaping time) and digitized. ^{57}Co, ^{22}Na and ^{137}Cs gamma ray sources were used for these measurements.

In order to assess the imaging potential of the continuous CsI(Tl)-PD combination, we used a 23 mm x 10 mm x 6 mm CsI(Tl) crystal, two PDs, and uncollimated gamma ray sources. The crystal was wrapped (top and sides) in 5 layers of teflon tape and coupled to the two PDs with optical grease. The PDs were attached to two available charge sensitive preamplifiers (ORTEC 142A and 109A). A 1-D weighted mean of the two PD signals determined the location of a gamma ray interaction.

III. RESULTS

A. The PSPMT Positioning Linearity, Resolution, and Imaging Capabilities

Figure 2 and 3 shows the results of stepping a 1.2 mm ^{57}Co slit source across the face of the NaI(Tl)-PSPMT device in 5 mm steps. Figure 2a displays the ratio positioning response in the x and y-direction. The extent of the linearity and dynamic range appear to give a central 5 x 5 cm useful FOV. The x-direction Line Spread Functions (LSFs) are

shown in Figure 2b. The FWHM spread of the LSFs is a measure of the camera's intrinsic resolution. The mean, standard deviation and range (max-min) of the FWHMs are, respectively, 2.6, 0.1 and 0.5 mm in the x-direction and 2.5, 0.2, and 0.6 mm in the y-direction. A simple deconvolution of the source size yields 2.3 and 2.2 mm FWHM for the mean intrinsic resolution in the x- and y-directions, respectively. These values should be compared to the standard gamma camera which has >3.5 mm FWHM intrinsic resolution.

Figure 3 shows the sum of the line images used to obtain the X LSFs (without flood correction) and the corresponding flood field image. The flood image shows the presence of hot spots on the image borders due to background from scattered gamma rays and noise. Within the inner, most linear 5 cm x 5 cm FOV, the standard deviation (σ) of the pixel intensity values in the flood image is 21% of the mean. In both cases the images span the size of the 60 x 60 mm^2 NaI(Tl) crystal area. The cause of the slant distortion in the upper right hand corner of the images is most likely due to the poor quantum efficiency of the photocathode in that region.

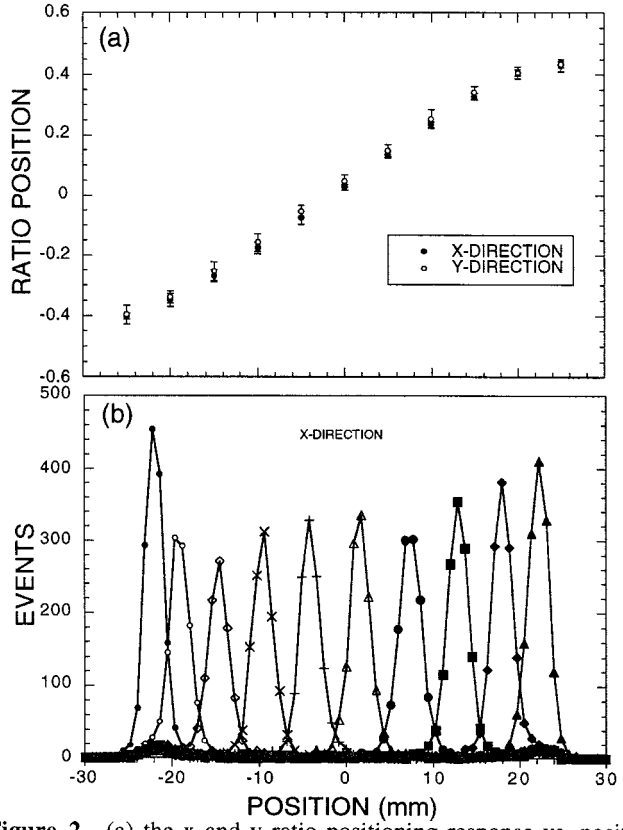

Figure 2. (a) the x and y ratio positioning response vs. position of a ~1.2 mm slit source of ^{57}Co stepped across the camera field of view in 5 mm steps; (b) the x- direction LSFs for NaI(Tl)-PSPMT.

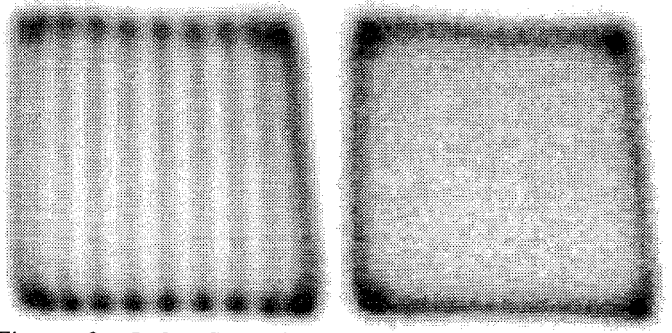

Figure 3. Left: Sum of the images used to obtain x-LSFs (without flood correction). Right: flood field image.

Figure 4a shows the resolution and sensitivity (measured with a ^{57}Co point source at the camera center) vs. length of the lead collimator holes used on the NaI(Tl)/PSPMT device. The collimator hole diameter was approximately 1.3 mm and the septa thickness was roughly 0.16 mm. Results in Figure 4a indicate that it may be possible to use less than the standard 4.0 cm thickness collimator, increasing sensitivity without much loss in resolution. The measured point source sensitivity at the center of the crystal, without the collimator, was approximately 4 x 10^4 counts/sec/μCi. With the 2.0 cm thick collimator the corresponding value was ~400 cts/sec/μCi. The measured resolution and sensitivity data are within 10% of that calculated using the standard collimator formulas for resolution and sensitivity vs. hole length.

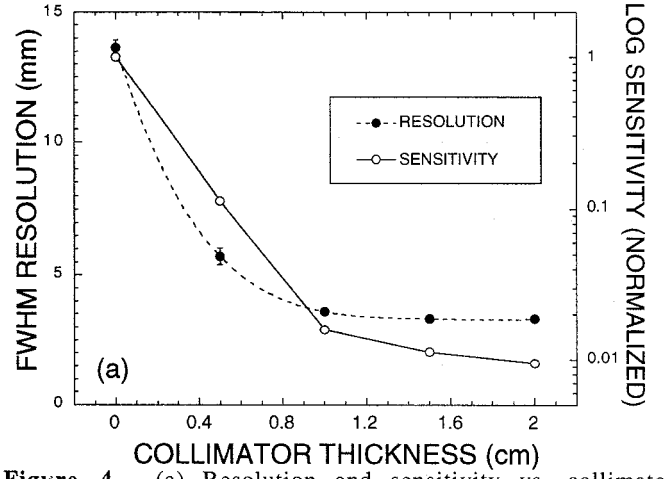

Figure 4. (a) Resolution and sensitivity vs. collimator thickness for NaI(Tl)-PSPMT for ^{57}Co point source at FOV center.

The image resolution (FWHM) of a ^{57}Co point source within a tissue equivalent scatter medium (Lucite sheets) was also measured. This simulates imaging a hot tumor within a cold compressed breast of different thickness. For all depths within scatter medium studied (0 - 45 mm thick), the point source was clearly resolved (3.0 - 7.5 mm FWHM).

Figures 5 and 6 show the high resolution imaging capabilities of the NaI(Tl)-PSPMT camera. Figure 5 (left) displays the digitized transmission phantom (scale shown). The letters have nominally 1.5 mm line widths (with some variation). Figure 5 (right) shows the corresponding image acquired with the NaI(Tl)-PSPMT camera using ^{99m}Tc. Figure 6 (left) shows a digitized small monkey brain phantom (Lucite; scale shown). Figure 6 (right) demonstrates that the NaI(Tl)-PSPMT camera with a 2 cm thick collimator is able to resolve some of the fine structures of this phantom (filled inside black bordered regions with ^{99m}Tc) with good linearity.

Figure 7 shows some of the results obtained with discrete crystal arrays coupled to the PSPMT. ^{99m}Tc flood irradiation histograms are displayed for arrays of (a) 2x2x6 mm^3 NaI(Tl) crystals spaced 0.5 mm apart and (b) 2x2x4 mm^3 CsI(Tl) crystals spaced 0.5 mm apart. Below each image is the extracted energy spectra from the crystal in row 2 and column 2 of each array (without gain corrections applied to the tube). A comparison between the two array results is difficult since there is a 3 mm glass window on the NaI(Tl) array and none for the CsI(Tl) array (there is also a 3 mm glass entrance window on the PSPMT). Cs or I escape x-rays results in a low energy asymmetry seen on the photopeaks.

The bottom graph of Figure 7 shows the results of stepping the 4 x 4 NaI(Tl) array across the PSPMT in 10 mm steps. We plot the ratio positioning response (crystal peak position in image) vs. actual crystal position for all array po-

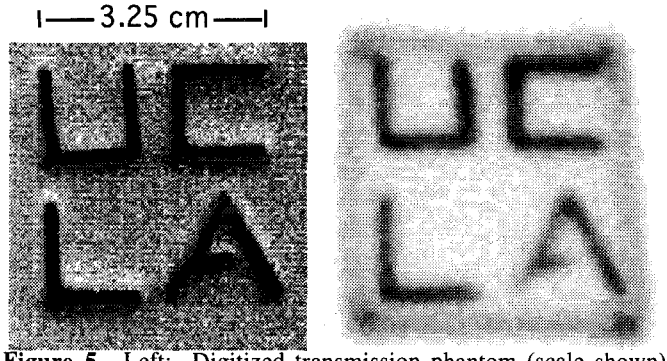

Figure 5. Left: Digitized transmission phantom (scale shown). Right: The corresponding image acquired with the NaI(Tl)-PSPMT camera (without flood correction) and ^{99m}Tc .

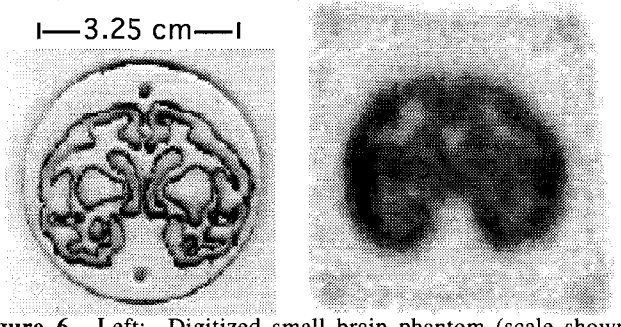

Figure 6. Left: Digitized small brain phantom (scale shown). Right: the NaI(Tl)-PSPMT camera has capability of resolving fine structures when the phantom is filled (inside black bordered regions) with ^{99m}Tc. Image is shown without flood correction.

sitions. The linearity and dynamic range appear to give a central 6 x 6 cm FOV, which is an improvement over the continuous crystal (see Fig. 2, for comparison and the end of section IIA). Imaging with the discrete array is accomplished by determining which crystal is hit and placing the event at that crystal location. A digital positioning mask made of the horizontal and vertical crystal borders in the flood image facilitates the decision of which crystal is hit. Results from imaging crystal arrays indicate that the intrinsic position resolution is determined by the size of the crystals in the array.

B. The PD Camera Simulations, Energy Measurements and Positioning Studies

Figure 8 displays some of the Monte Carlo results for the continuous crystal CsI(Tl)-photodiode design (Fig. 1a). The top of Figure 8 shows Monte Carlo simulations of scintillator light spread aperture (FWHM and FWTM) for a point source of light at the center of a CsI(Tl) crystal as a function of light diffuser thickness. A ^{99m}Tc 140 keV gamma ray photoabsorption in CsI(Tl) will create approximately 7300 scintillation photons, on average. These optical photons were tracked and the spread of light across the detector face determined. A PD quantum efficiency of 75% was assumed. For a 4 mm thick light guide, the predicted FWHM spread, (~11 mm) is roughly the size of the proposed photodiode spacing, which is appropriate for event positioning. The bottom of Figure 8 shows results of Monte Carlo simulations of intrinsic position resolution (fluctuation in scintillation event positioning) as a function of depth within crystal of a point source origin of light (depth of interaction). Resolution is predicted with and without estimated weighted mean positioning errors due to photodiode noise and size error propagation. We see from the figure that intrinsic resolution better than 2.0 mm FWHM is expected at the center for all depths of interaction. The attainable system resolution will, of course, be further limited by the collimator properties.

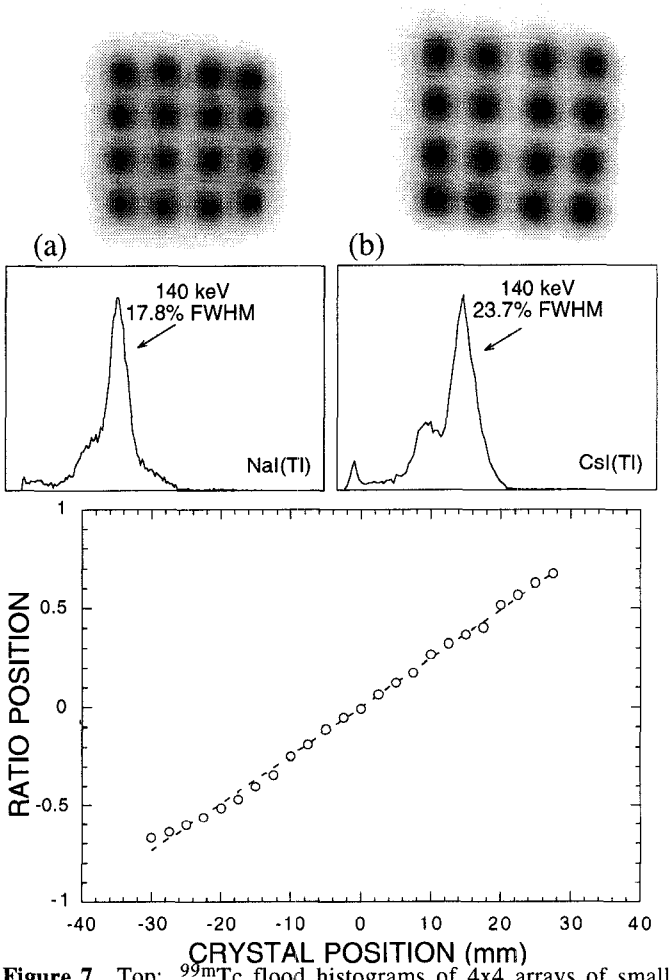

Figure 7. Top: ^{99m}Tc flood histograms of 4x4 arrays of small (a) NaI(Tl) and (b) CsI(Tl) crystals. Below each image is extracted energy spectra from the crystal in row 2 and column 2. Bottom: ratio positioning response for each crystal position in the 4x 4 NaI(Tl) array when translated across the PSPMT in 10 mm steps.

Figure 9 shows measurements of typical energy resolution capabilities of the proposed CsI(Tl)-PD combination (1 cm^2 PD). In all cases, we fit the measured photopeak to a single gaussian (which is inappropriate for the ^{57}Co data because of a higher energy line at 136 keV and the presence of the ~90 keV x-ray escape peak, seen in Fig.7). An energy resolution of (a) 23, (b) 8.9 and (c) 7.6% FWHM was measured for the 122, 511, and 662 keV lines of ^{57}Co, ^{22}Na and ^{137}Cs sources, respectively. The ^{57}Co gamma ray energy is similar to that emitted from ^{99m}Tc (the amplifier gain of the measured ^{57}Co spectrum was a factor of 3.33 higher than for the other two spectra). Due to the good match between the CsI(Tl) emission and silicon absorption spectra, relatively good energy resolution characteristics are seen even in the presence of a PD dark current of 2-5 nA and a terminal capacitance of 40 pf. These results would significantly improve if the area of the photodiode were smaller and better matched to the small CsI(Tl) crystal used.

We performed an approximate charge calibration using the electronic pulser test input of the preamp. The total noise contribution for this PD-preamplifier combination was determined to be approximately 450 electrons RMS . The ^{57}Co 122 keV peak corresponds to roughly 3900 photoelectrons. Assuming a photodiode quantum efficiency of roughly 75%, this is equivalent to 5200 scintillation photons input to the PD. A 122 keV gamma ray interaction in CsI(Tl) should produce ~6300 scintillation photons, so that we are

collecting ~82% of the available scintillation light. This fraction compares well to that calculated from DETECT Monte Carlo photon tracking studies. The 122 keV peak channel in Figure 9 is nearly twice the top channel of the noise shoulder. This SNR is sufficient for good positioning characteristics.

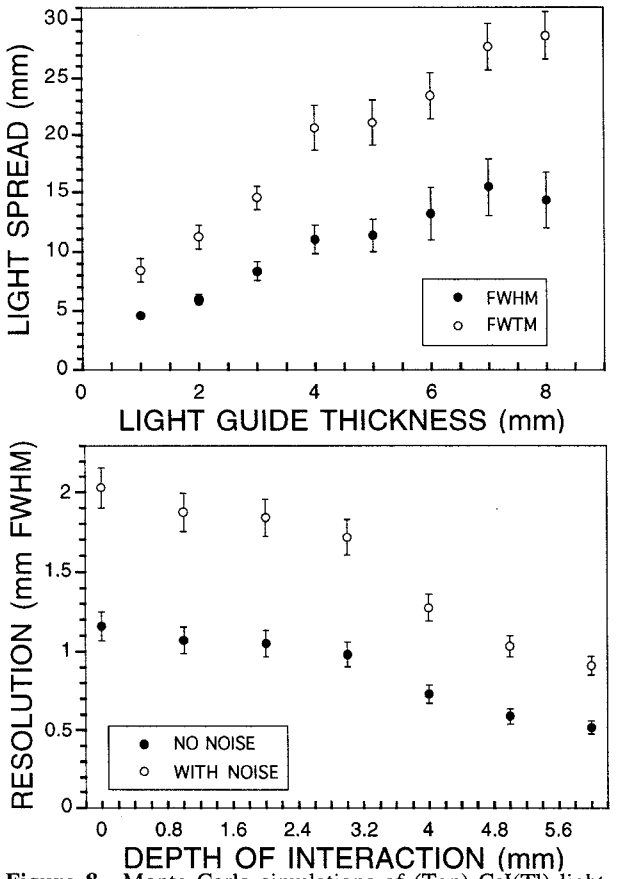

Figure 8. Monte Carlo simulations of (Top) CsI(Tl) light spread (FWHM and FWTM) as a function of light diffuser thickness and (Bottom) intrinsic position resolution vs. interaction depth within crystal . Resolution is predicted with and without estimated weighted mean positioning errors due to PD noise and size.

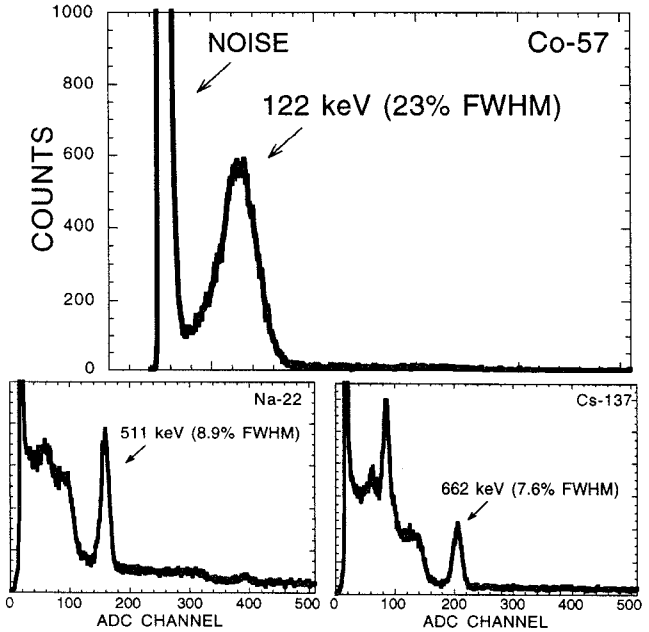

Figure 9. Energy spectra measured with a 2x2x10mm^3 CsI(Tl) crystal, a 1cm^2 PD, and ^{57}Co, ^{22}Na and ^{137}Cs gamma ray sources.

IV. SUMMARY

A small scintillation camera may be very useful in imaging the breast because it allows for optimum camera positioning and can take advantage of the use of breast compression. We have considered the position sensitive PMT (PSPMT) with NaI(Tl), and the silicon PIN photodiode(PD) with CsI(Tl). The former has the advantage of high signal-to-noise ratio and gain. The latter has an advantage in terms of compactness and eventual cost. We have achieved intrinsic resolution of 2.2 mm FWHM with the PSPMT scheme. We have seen that there is adequate signal-to-noise ratio in the PD design for gamma ray event positioning. Future studies will also include a more detailed comparison between the discrete and continuous crystal geometries, and efforts to improve the dynamic range and resolution of the PSPMT readout. As a final note, the silicon Avalanche Photodiode (APD) is also ideal to readout CsI(Tl). However, as of yet, no reliable APD array is available.

V. ACKNOWLEDGMENTS

This work was supported in part by funds provided by the Breast Cancer Fund of the State of California through the Breast Cancer Research Program of the University of California, Grant Number IRB-0225, the Department of Energy (DE-FCO3-87-ER60615), National Institutes of Health (RO1-CA61037), and a pilot research grant from the Society of Nuclear Medicine Education and Research Foundation.

VI. REFERENCES

[1] C.J. Thompson, K. Murthy et.al. "Positron Emission Mammography (PEM): A Promising Technique for Detecting Breast Cancer." IEEE Trans. Nucl. Sci, 42-4:1012-7 (1995).

[2] W.W. Moses, T.F. Budinger, R.H. Huesman and S.E. Derenzo. "PET Camera Designs for Imaging Breast Cancer and Axillary Lymph Node Involvement." J. Nucl. Med. 36-5:69P, May 1995.

[3] G.D. Hutchins and A.J. Simon. "Evaluation of Prototype Geometries for Breast Imaging with PET Radiopharmaceuticals." J. Nucl. Med 36-5:69P, May 1995.

[4] B.E. Patt, J.S. Iwanczyk, Y.J. Wang, M.P. Tornai, C.S. Levin, E.J. Hoffman. "Mercuric Iodide Photodetector Arrays for Gamma-Ray Imaging." *Nucl. Inst. & Meth. A* (in press).

[5] J.N. Aarsovold, H.H. Barrett, et. al. "Modular scintillation cameras: a progress report." Proc. SPIE. 914(A):319-25.

[6] A.J. Bird, et.al. "Multi-channel readout of crossed wire anode photomultiplier." Nuc Inst Meth A348(2-3):668-72 (1994).

[7] N.J. Yasillo, R.N. Beck, M. Cooper. "Design considerations for a single tube gamma camera." IEEE Trans. Nucl. Sci. 37(2):609-15 (1990).

[8] Weisenberger, A.G.; Majewski, S.; Mehrotra, S.; Popov, V.; and others. Investigation into the use of position sensitive photomultiplier tubes for beta radiography. 1994 IEEE Nucl. Sci. Symp. Conf. Rec 1:351-5 (1995).

[9] E. Rossi, C. Labanti, et al. "A hexagonal multi-element CsI(Tl)-photodiode module for gamma-ray imaging." 1995 Conf. Rec. IEEE Nuc. Sci. Symp. 1:60-64 (1995).

[10] T. Carter et al. " An imager prototype for gamma-ray astronomy." 1994 IEEE Nucl Sci Symp Conf Rec 1:56-59.

[11] C.S. Levin, E.J. Hoffman, M.P. Tornai, L.R. MacDonald. "Design of a Small Scintillation Camera with Photodiode Readout for Imaging Malignant Breast Tumors." J. Nucl. Med. 37, p. 52, May 1996.

[12] GF Knoll, TF Knoll, TM Henderson. "Light Collection in Scintillating Detector Composites for Neutron Detection." IEEE Trans. Nucl. Sci. NS-35(1):872-5 (1988).

[13] S Siegel, RW Silverman, Y Shao, SR Cherry. "Simple Charge Division Readouts for Imaging Scintillator Arrays Using a Multi-Channel PMT." IEEE Trans. Nuc. Sci. NS-43: 1634-41 (1996).